Piezoelectric and microfluidic tuning of an infrared cavity for vibrational polariton studies

Wei Wang, Jaime de la Fuente Diez, Nicolas Delsuc, Juan Peng, Riccardo Spezia, Rodolphe Vuilleumier, Yong Chen

ARTICLE

Received 00th January 20xx,
Accepted 00th January 20xx

DOI: 10.1039/x0xx00000x

Piezoelectric and microfluidic tuning of infrared for vibrational polariton studies

Wei Wang,[a] Jaime de la Fuente Diez,[a] Nicolas Delsuc, [a] Juan Peng,[a] Riccardo Spezia, [b] Rodolphe Vuilleumier, [a] and Yong Chen*[a]

We developed a microfluidic system for vibrational polariton studies, which consists of two microfluidic chips: one for solution mixing and another for tuning an infrared cavity made of a pair of gold mirrors and a PDMS spacer. We show that the cavity of the system can be accurately tuned with either piezoelectric actuators or microflow-induced pressure to result in resonant coupling between a cavity mode and a variational mode of the solution molecules. Acrylonitrile solutions were chosen to proove the concept of variational strong coupling (VSC) of a C≡N stretching mode with light inside the cavity. We also show that the Rabi splitting energy is linearly propertional to the square root of molecular concentration, thereby providing the relevance and reliability of the system for VSC studies.

Introduction

Molecular variational polaritons are hybrid states arising from resonant coupling between a molecular vibration mode and an infrared cavity mode [1]. Under strong coupling regime, the polariton-mediated chemistry might be significantly different from the conventional ones [2–5]. To understand clearly how a chemical reaction is affected by polariton kinetics or vibrational strong coupling (VSC), more systematic investigations, both theoretically and experimentally, are needed. [6–14] Despite the intense efforts during the last years, [15–20] there is still open important open questions and there is no general method for flexible and easy tuning of the cavity mode and other experimental parameters. The reproducibility of some enhanced chemical reactions, for instance, is currently under debate [21,22] and most previous studies have been performed using a cavity made of a stainless steel cell and a high-stiffness spacer.[23-27]

Generally speaking, the high accuracy cavity tuning is a central requirement for VSC studies. Several groups have recently developed cavity tuning methods by using different types of piezoelectric actuators.[21,22,28] Mochalov et al.[29] used a piezo-positioner, an XY-stage, and a microscope objective to find a resonant area of a cavity formed with a plane and a convex mirror. This study is interesting but it has not been used for polariton studies. Imperatore et al. [21] developed a cavity with a pair of gold mirrors on sapphire optical windows mounted on a piezo-controlled translation stage that enables manual movement over a wide range with 1 µm resolution and piezoelectric actuation over a 20 µm range with 0.6 nm resolution. By using this system, they reproduced the vacuum Rabi splitting of cyanate ion hydrolysis reported by Hiura et al.[30] but failed to observe any change in the reaction rate. Thus, this work argued for a broader effort to independently reproduce more of these claims by considering much enthusiasm and speculation in the field. Wiesehan et al also attempted to reproduce cavity catalysis but did not observe the increase of in the reaction rate constant reported by Lather et al[31], suggesting that cavity catalysis is sensitive to the experimental details beyond the onset of vibrational strong coupling. Finally, Hirai et al.[28] developed a piezoelectric system with a computer-controlled feedback loop for automatically tuning the cavity to maintain VSC with a target vibrational mode throughout the course of a reaction which may change the refractive index within the cavity. In summary, previous techniques with piezoelectric actuators were more flexible than using stainless steel cells but they were still limited to the use of rigid spacers or without dynamic control of the flow.

Surprisingly, perhaps, there is no report on microfluidic cavity tuning of vibrational polaritons. Microfluidic technologies have been developed for more than two decades and a large variety

[a] *École Normale Supérieure-PSL Research University, Département de Chimie, Sorbonne Universités-UPMC Univ Paris 06, CNRS UMR 8640, PASTEUR, 24, rue Lhomond, 75005 Paris, France. Email: yong.chen@ens.psl.eu*

[b] *Laboratoire de Chimie Théorique, UMR 7616 CNRS, Sorbonne Université, 4, place Jussieu, 75252 Paris Cedex 05 - France*

Electronic Supplementary Information (ESI) available: [details of any supplementary information available should be included here]. See DOI: 10.1039/x0xx00000x

of tools and techniques are now available for the dynamic control of microflows, including mixing, hydrodynamic focusing, concentration changing, concentration gradient generation, and real-time monitoring.[32] The application of microfluidic techniques to the variational polariton studies should be interesting not only for polariton chemistry of high production rate due to continuous flow but also for its flexibility in flow dynamics. Nevertheless, the cavity modes are highly sensitive to the environmental changes caused by the flow and it is preferable to add an independent chip upstream of the cavity chip.

In this work, we developed a piezoelectric and microfluidic tuning method to study the vibrational polaritons. While piezoelectric tuning is able to modify the cavity length with high precision, microfluidic tuning can be applied to tune a cavity made of a pair of two rigid mirrors and an elastomeric spacer such as polymethylsiloxane (PDMS). This is because of the fact that at a constant flowrate the pressure in the cavity area can be sufficiently large to push away the two mirrors due to the low Young's modulus of PDMS. By using an acrylonitrile-filled cavity, we demonstrate that both piezoelectric and microfluidic tuning are capable of setting a resonant coupling of molecular vibrational and cavity photonic modes. With the help of the upstream mixing chip, solutions at different acrylonitrile concentrations are prepared for the observation of the linear relationship of the resulting Rabi splitting and the square root of the molecular concentration. Numerical simulations are also performed to semi-quantitatively interpret the experimental results, showing a consistent ability of the system for the vibrational polariton studies.

Methods

All spectra were collected with an Agilent Cary 600 FTIR spectrometer (Agilent, France) and a homemade microfluidic module consisting of a solution mixing chip, a cavity chip with two piezoelectric actuators, and accessories. While the solution flowing in the cavity is prepared upstream in the mixing chip with the two syringe pumps (Fig. 1a), the cavity length can be tuned with two piezoelectric actuators. The cavity chip is made of a pair of CaF_2 plates (Tianjin Tianguang Optical Instrument Co., Ltd., China) coated with 10 nm thick Au film and 20 nm Parylene C, and a patterned PDMS spacer with channels (Fig. 1b). Here, Parylene C films are used to protect the gold layer from possible contamination of chemical reagents. For the convenience of operation, the mixing and cavity chips are mounted on two sides of a metallic support (Fig.1c, 1d). The cavity chip itself is sandwiched by two metallic plates with circular openings and withstood with two piezoelectric actuators (#P-841.20, PI, Germany). This microfluidic unit, except the two syringe pumps, is installed inside the spectrometer which can be moved and rotated horizontally with differential screw translators. More details of the microfluidic unit handling and the overlay of the two chips are shown in Fig. S1 and Fig. S2.

Fig.1e and 1f show photographs of a mixing chip and a cavity chip before assembling. The PDMS spacer of the cavity chip was produced by casting a liquid PDMS mixture against a photolithography-defined mold, which was patterned with a layer of AZ photoresist (Microchem. France) spun coated on glass (2500 rpm, 40s) and baked at 120°C on a hotplate for 1 min before exposure. After resist development and exposure to trimethylchlorosilane (TMCS, Sigma, France) vapor, a mixture of PDMS pre-polymer and crosslinker (GE RTV 615, France) at a ratio of 10:1 was spun-coated at 3500 rpm for 10 min. on the resist layer, and baked at 120°C for 30 min. After cooling down to room temperature, the sample was immersed in ethanol to dissolve the remaining AZ resist and a small piece of PDMS membrane was gently lifted off and floated on the top of ethanol solution. To fabricate the mixing chip, SU8-3050 (MicroChem, France) was spun coated on a glass slide at 1000rpm for 40s and baked at 95°C for 3 h. Then, it was exposed by UV light for 15 s through a mask containing a Y-channel and a serpentine pipeline, and baked at 95°C for 20 min. Afterward, it was covered with a 100 µm thick PDMS film and a plastic plate with female Luer connectors.

The preliminary parallelism of the cavity was obtained by adjusting 6 hand nuts on the screws fixed on one of the metallic plates with a circular opening until the appearance of concentric Newton's rings, indicating a negligible thickness variation across the center of the cavity probed by the FTIR beam. The two piezoelectric actuators were mounted with a metallic plate pre-fixed on the vertical support. Then, they were carefully regulated against the cavity chip. In addition, a grating marker was added to align the optical window with the transmitted light spot consistently for each experiment. The two chips as well as the two syringe pumps were connected with standard Luer elements. To prevent chemical corrosion or modification, all fluid contact materials were coated with 20 nm of Parylene C. Finally, analytical grade acrylonitrile, heptane, and other chemicals (Sigma-Aldrich, France) were used in this work and both flowrate and concentration in the cavity were regulated by adjusting the pulling speed of the syringe pumps. Since the flow resistance of an IR cavity can be high, particular attention was paid to the cavity stability during the fine tuning in order to achieve high-quality measurements.

Numerical calculations were performed by using a transfer matrix method[32], the dielectric constant of CaF_2[33] , the frequency-dependent dielectric constant of Au[34], and other parameters of the system by design or experimentally determined. Python scripts were prepared for simulations and parametric fitting of the experimental data.

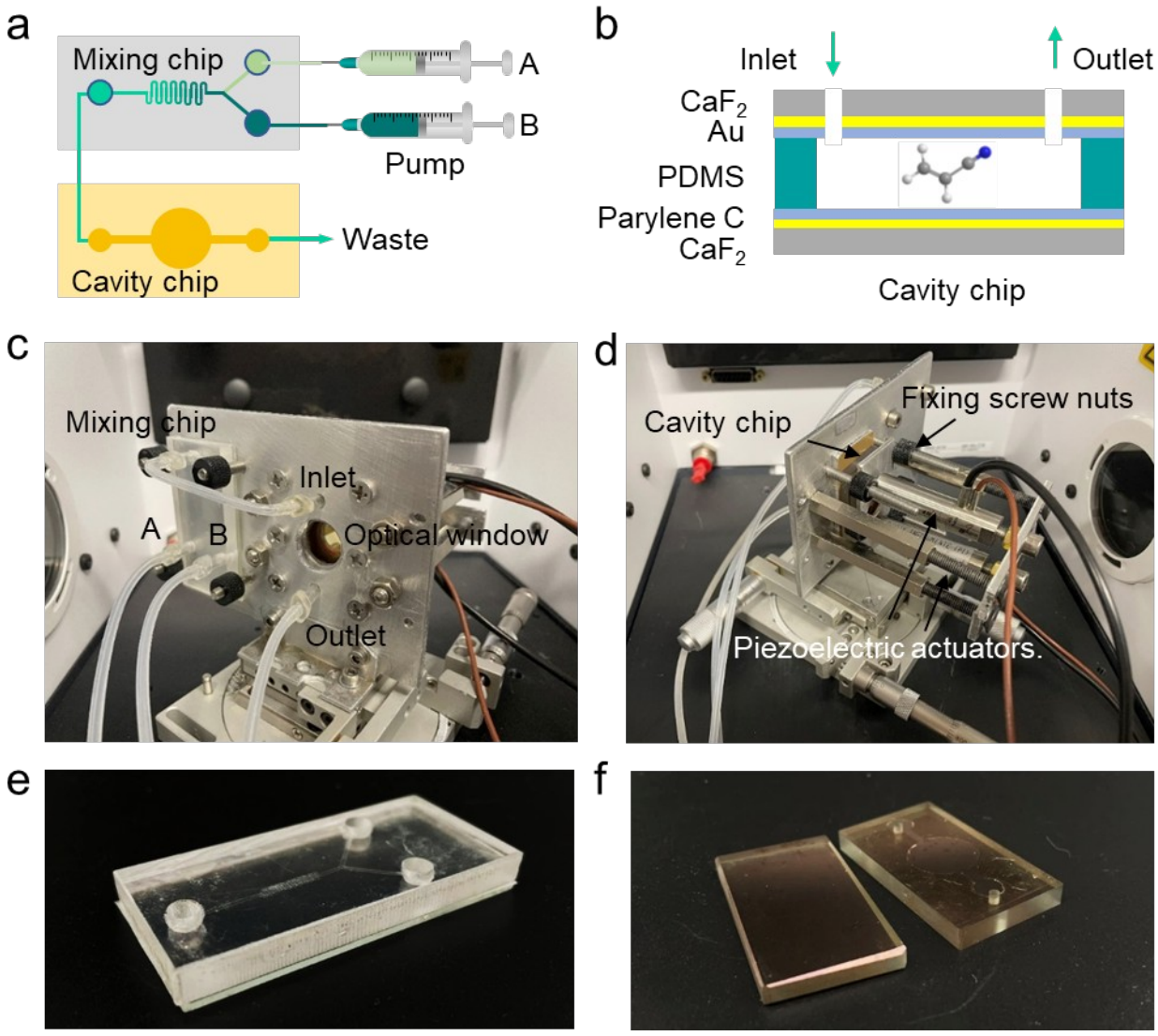

Figure 1. Experimental setup for vibrational polariton studies. (a) Schematic of the setup consisting of a mixing chip, a cavity chip, and two syringe pumps. (b) Cavity chip made of a pair of gold and Parylene coated CaF_2 plates and a patterned PDMS spacer. (c, d) Photographs of the setup mounted inside a FTIR spectrometer. For the convenience of operation, the mixing chip and the cavity chip are mounted on two sides of metallic support, which can be moved and rotated horizontally with differential screw translators. The cavity chip is sandwiched with two metallic plates with openings and withstood with two piezoelectric actuators. (e) Mixing chip made of a plastic plate, a PDMS buffer layer, and a glass slide with patterned SU8 resist. (f) Cavity chip before assembling.

Results and discussion

Piezoelectric tuning of cavity modes

Fig.2 shows the typical IR transmission spectra of the air- and water-filled cavities. The A and B spectra are recorded with a bare cavity of different cavity lengths. Since the wave number of the m[th] cavity mode is given by $\tilde{\nu}_m = m/2n_S L_c$, the cavity length L_c can be deduced from n_S, the refractive index of air (1.0), and the peak positions of A and B spectra. Thus, the deduced cavity lengths of A and B are 14.8 µm and 14.3 µm, respectively. The full width at half maximum (FWHM) and the free spectral range (FSR) of the spectra A and B can also be calculated, i.e., FWHM = 16 cm^{-1} and 20 cm^{-1} and FSR = 337 cm^{-1} and 349 cm^{-1}, respectively. Accordingly, a cavity Q-factor of 21 (A) and 17 (B) can be estimated, respectively. Fig. S3 shows a comparison of the experimental and theoretical transmission spectra of an air-filled cavity over a large range of wavenumber, with and without piezoelectric tuning. Here, the same cavity lengths deduced from experimental data (14.8 µm and 14.3 µm were used for simulation with a pair of 10 nm thick Au mirrors and the dielectric constant of Au reported previously [34].

Fig. 2b illustrates the piezoelectric tuning accuracy. As can be seen, the cavity mode can be tuned toward low or high wavenumbers with an accuracy of 5 cm^{-1}, which corresponds

to a length tuning accuracy of 35.7 nm. Accordingly, a thickness variation of about 1.2 µm should be able to cover half of the FSR. For a PDMS spacer of 14.5 µm, this is achievable by 8% deformation of the PDMS layer. Therefore, if the initial setting is within the limit of elastic deformation of PDMS, fine-tuning of the cavity length can be repeated piezoelectrically. This also allowed to generate high resolution differential spectra as shown in Fig. S4.

The angle-dependent transmission spectra of the air- and water-filled cavities are shown in Fig. 2c and 2d. The spectra of the air-filled cavity display the progression of the cavity modes as a result of interference between the two mirrors, which can be calculated by using [35]

$$T_e = \frac{(1-R)^2}{1-2R\cos\delta + R^2} \quad (1)$$

$$\delta = \left(\frac{2\pi}{\lambda}\right) 2 n_S L_{ca} \cos\theta \quad (2)$$

where T_e is the transmittance function, δ is the phase difference between each successive transmission pair, R is the reflections of the mirror, θ is the incident angle of light, and λ is the wavelength of light. Clearly, the in-plane wave vector for a given angle of incident light determines the peak position of the resonance in the cavity. As the angle increases, the optical path becomes larger, which results in a redshift of the peak. More precisely, λ increases and the wavenumber decreases with the increase of θ. When the cavity is filled with water, similar redshifts are observed with the resonance peaks. However, the magnitude of the redshift of the water-filled cavity is smaller than that of the air-filled cavity, and the FSR also became smaller, due to the higher refractive index of water ($n_{water} = 1.333$).

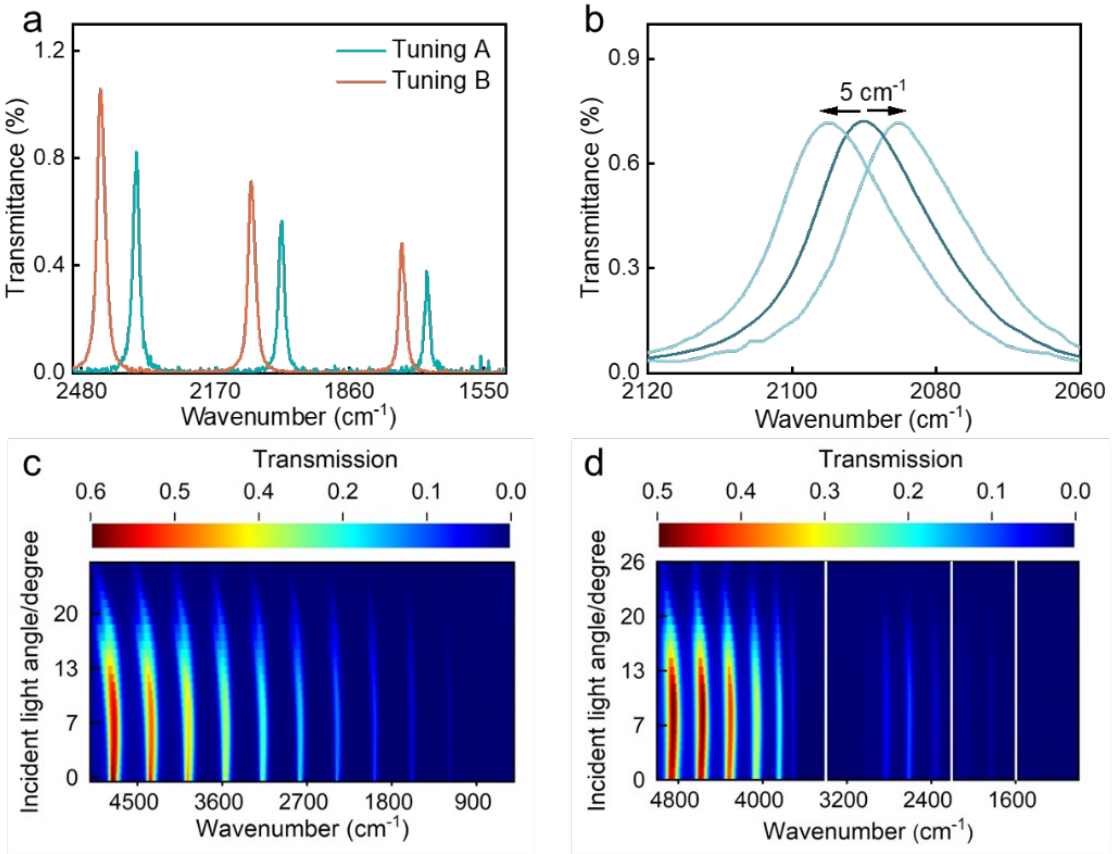

Figure 2. (a) Piezoelectric tuning of transmission spectra of a bare Fabry-Perot, corresponding to a cavity length of 14.8 µm (A) and 14.3 µm (B), respectively. (b) Piezoelectric tuning of a cavity mode with a tuning accuracy of 5 cm^{-1}. (c, d) Angle-dependent spectra of an air-filled cavity and a water-filled cavity. White lines represent the O-H stretching vibration (3400 cm^{-1}), the cooperative hydrogen bond vibration (~2200 cm^{-1}), and the bending vibration (1600 cm^{-1}) of vibrational modes of H_2O, respectively.

Piezoelectric tuning of polaritons

Figure 3a shows a typical transmission spectrum of an acrylonitrile-filled cavity tuned to a C≡N stretch mode. In addition to the regularly spaced cavity modes, a doublet appears around 2229 cm^{-1} due to Rabi splitting of vacuum strong coupling of cavity mode and molecular vibration (cavity mode m=6, 2227 cm^{-1}). The insert of Fig. 3a schematically

shows the energy levels of molecular vibration modes, a cavity mode, and polaritons with a Rabi splitting of $\hbar\Omega_R$. Fig. 3b shows in more detail the doublet of a piezoelectrically tuned (blue) and slightly detuned (orange) cavity in comparison with the transmission spectrum of acrylonitrile without cavity (black). The chemical structure of acrylonitrile in the ball-and-stick model is also shown.

As expected, the piezoelectric cavity tuning is efficient for studies of vibrational polaritons. In the case of strong coupling, the energy exchange between photons and vibrating molecules should be faster than the dissipative channel, resulting in two hybrid light-matter states. More generally, the wave functions of these two polariton states can be expressed as follows, [36]

¿ (3a)

¿ (3b)

where $|e,0\rangle$ denotes an *e*xcited state of molecular vibration with 0 photons, $|g,1\rangle$ denotes a *g*round state of molecular vibration with 1 photon, α and β are coefficients of the probabilities. When photon and molecular vibration energies are equal, the polaritons are 50-50 quantum superpositions of photon and molecular vibration, with Rabi splitting energy between the upper ($P^{+¿¿}$) and the lower ($P^{-¿¿}$ polaritons. According to the Jaynes-Cummings two-state model, the Rabi splitting is related to a number of variables such as dissipation: [37–40]

$$\hbar\Omega_R=\sqrt{4G^2-(\gamma_M-\gamma_C)^2} \quad (4)$$

where *G* is the coupling strength parameter, γ_M and γ_C are the linewidths of uncoupled vibrational and cavity photon states, respectively. By definition, γ_M and γ_C are related to the decay constants of the two states ($\gamma=\hbar/\tau$). Without dissipation, the Rabi splitting becomes

$$\hbar\Omega_R=2G=2d\sqrt{N}\sqrt{\frac{\hbar\omega}{2\epsilon_0 v}}\sqrt{n_{ph}+1} \quad (5)$$

where d is the transition dipole moment of a single molecule, *N* is the number of molecules, $\hbar\omega$ is the resonant energy, ϵ_0 is the vacuum permittivity, *v* is the mode volume of the cavity, and n_{ph} the number of photons involved in the coupling. Clearly, a Rabi splitting remains even without photon (n_{ph}=0), meaning that the molecules still interact with the cavity in the absence of incident light.

The stretching vibration mode of the acrylonitrile C≡N bond has been chosen because of its suitability of IR frequency (2229 cm^{-1}) and its relatively high oscillation strength. Experimentally, a solution of acrylonitrile molecules was prepared in the mixing chip and injected into the cavity chip. Then, the cavity length was tuned with the two piezoelectric actuators to reach two polaritons of equal height, i.e., the 50-50 quantum superpositions of photon and molecular vibration states in both upper and lower polaritons. While the Rabi splitting energy can be determined by measuring the frequency difference of the two peaks (39.2 cm^{-1}), the values of γ_M and γ_C are obtained by measuring the FWHM of the corresponding spectral peaks (15.4 cm^{-1} and 20.0 cm^{-1}).

Clearly, the measured Rabi splitting is much smaller than the FSR value of the cavity modes but significantly larger than the linewidths of uncoupled molecular vibration and cavity photon modes. According to Savona et al [35], the strong coupling limit is defined by $2G>\sqrt{\gamma_M^2+\gamma_C^2}$ ($2G=39.2\,cm^{-1}$, $\sqrt{\gamma_M^2+\gamma_C^2}=25.2\,cm^{-1}$), so that our piezoelectric tuned system is perfectly within the strong coupling limit.

By using the transfer matrix method [32] and the known parameters ($n_M=1.391$ for the refraction index of liquid acrylonitrile, 2229 cm^{-1} for the resonance wavenumber, and the frequency-dependent gold dielectric constant reported in the literature [34]), the polariton spectra could be simulated. As shown in Fig. S5, transmission spectra resembling the measured ones could be obtained by using the following adjustable parameters: cavity thickness = 9.85 μm (blue), 9.53 μm (orange), normalized coupling strength 4.5×10^{-4}, and linewidth = 8.0 cm^{-1}.

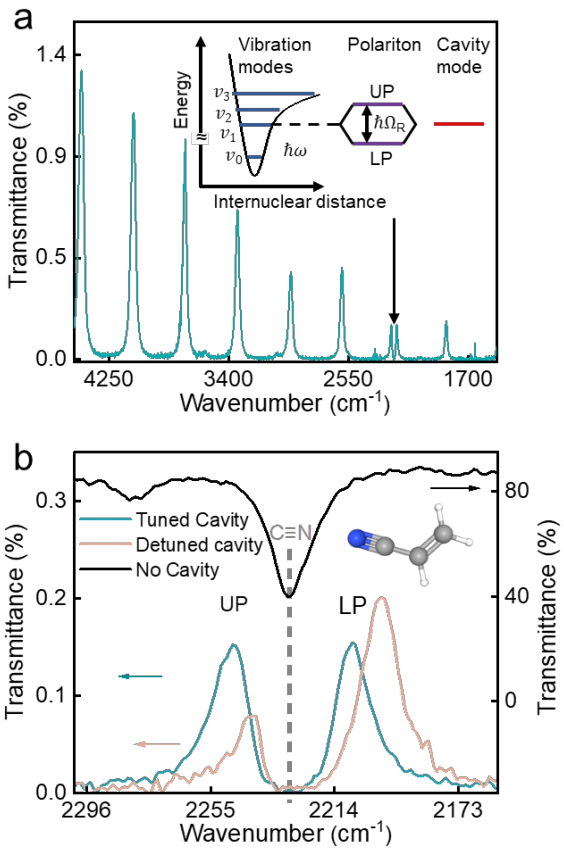

Figure 3. (a) Transmission spectrum when a cavity resonance is tuned to a C≡N stretch mode of acrylonitrile, showing regularly spaced cavity modes except for a doublet around 2229 cm^{-1} (polariton Rabi splitting). The insert schematically shows energy levels of molecular vibration modes, a cavity mode, and polaritons with a Rabi splitting ($\hbar\Omega_R$). (b) Zoomed spectra of tuned (blue) and slightly detuned (orange) doublet in

comparison with the transmission spectrum of acrylonitrile without cavity (black). The insert is the chemical structure of acrylonitrile in the ball-and-stick model.

Microfluidic tuning of polaritons

Fig. 4a shows the transmission spectra of an acrylonitrile-filled cavity at different flowrates. Clearly, both UP and LP peaks were redshifted with the increase of flowrate and the system was progressively detuned, showing two polariton branches of unequal heights. As expected, when the flowrate was switched off the polariton branches became again of equal heights. The flowrate-dependent cavity detuning can be explained by considering the steady-state Navier-Stokes equation:[41,42]

$$-\rho\vec{v}\vec{\nabla}\cdot\vec{v}+\mu\vec{\nabla}^2\vec{v}=\vec{\nabla}p \quad (6)$$

where ρ, $\vec{v}$, and μ are the density, speed, and viscosity of the fluid, respectively, p is applied pressure. For a rectangle channel with rigid walls, the Navier-Stokes equation can be reduced to

$$\Delta p=\frac{1}{1-0.63(\frac{L}{W})}\frac{12\mu}{L^3W}Q_c \quad (7)$$

Here, Δp is the pressure drop, L is the channel height (cavity length), W is the channel width, and Q_c is the flowrate. In our case, the upper and lower channel walls are rigid CaF_2 plates with a Young's modulus in the order of 10 GPa. Due to the much smaller Young's modulus of PDMS (in the order of 1 MPa), the pressure exercised on the two CaF_2 plates is capable of deforming the PDMS spacer and increasing the cavity length of the chip, as illustrated by Fig. 4b. Typically, with a flowrate of 10 µl/min, a fluid viscosity of 1cP, and a channel of 10 µm height, 3 mm width, and 29 mm cm length, a pressure of 1336 Pa should be applied. In turn, an average pressure in the order of 650 Pa can be approximated which can deform vertically the PDMS spacer for several nm. In practice, it is difficult to resolve Eq.7 for the deformation calculation of the PDMS spacer. By fitting the polariton energy shifts as a function of flowrate, we found a power law dependence between the flowrate and the cavity length, as shown in Fig. 4c. This can be expressed as,

$$L=L_0+\alpha Q_c^{\beta} \quad (8)$$

where L and L_0 are respectively the cavity length with and without flow, and α and β are two fitting parameters. By using the least square method, we obtained a fitting curve (orange) with α = 0.014 and β = 0.29.

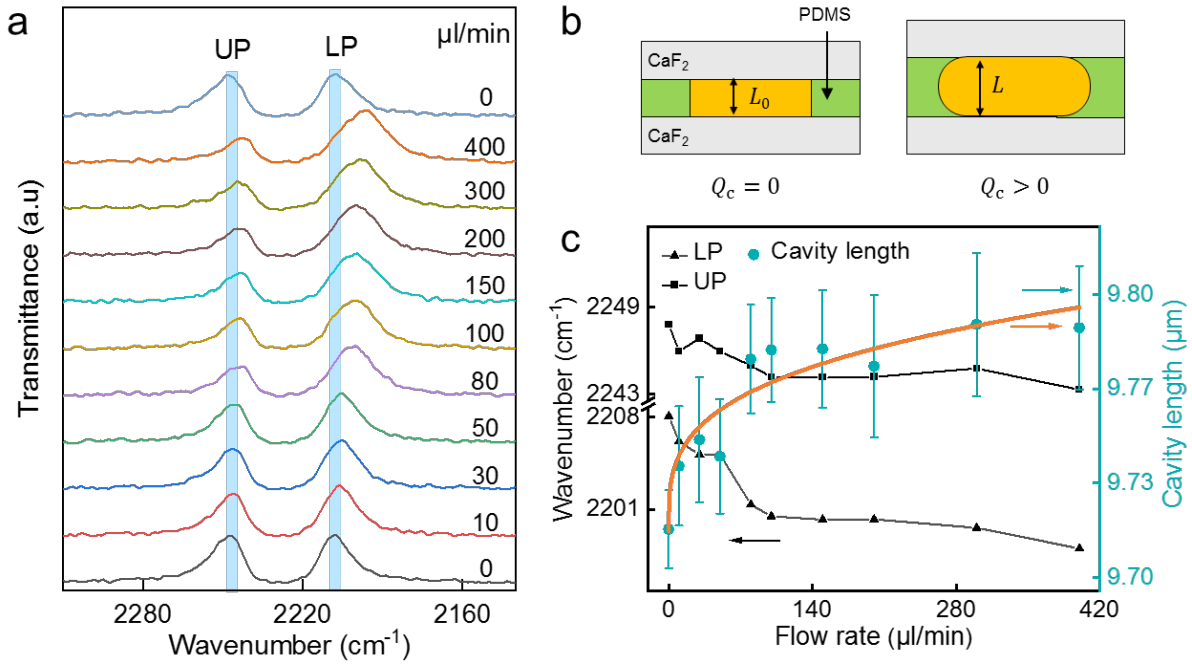

Figure 4. (a) Transmission spectra of an acrylonitrile-filled cavity at different flowrates, showing a redshift of both UP and LP peaks with the increase of flowrate. (b) Schematic diagram to explain the effect of flow induced red shift. According to the Navier-Stokes equation, increasing the flowrate reflects an increase of the pressure inside the cavity so that the cavity length can be increased due to the low Young's modulus of PDMS. (c) Variation of the cavity length as a function of flowrate, showing a power law dependence.

Fig. 5a shows the transmission spectra of an acrylonitrile-filled cavity obtained at a flowrate of 0 and 400µl/min with and without tuning. From bottom to top, the cavity polariton is slightly detuned at a flowrate of 400µl/min (orange). By using the piezoelectric actuators at the same flowrate, the polariton can be turned to reach two symmetric peaks (green). After switching off the flow, the cavity was detuned (brown) and then returned to symmetric states when the flow was switched on again (blue). This demonstrates the ability of microfluidic tuning of polariton states. Fig. 5b shows the microfluidic tuning by flow switching on, confirming the reliability of this method.

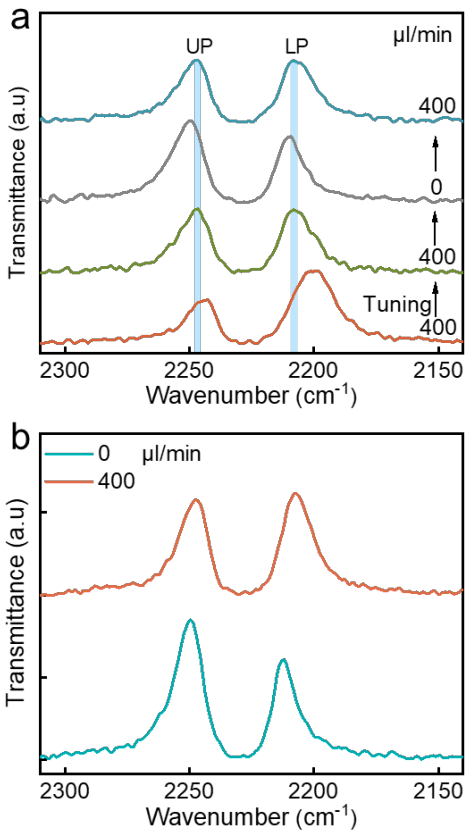

Figure 5. (a) Transmission spectra of an acrylonitrile-filled cavity obtained at different flowrates with and without tuning. From bottom to top, the cavity is slightly detuned at a flowrate of 400 µl/min (orange). Then, the cavity is tuned at the same flowrate by using the two piezoelectric activators (green). After switching off the flow, the cavity is detuned (brown). Finally, when the flow is switched on the cavity is tuned again (blue). (b) Flow induced tuning by the cavity.

Concentration dependence

Fig.6 shows the transmission spectra of an acrylonitrile-filled cavity at different concentrations (1.5-15 M) and the linear dependence of the observed Rabi splitting on the square root of acrylonitrile concentration. The fitting curve in Fig.6b is obtained by the least mean square method with R=0.91. Heptane ($n_{heptane}=1.386$) was used as a diluent because it is IR transparent at wavelengths in the vicinity of the C≡N stretching absorption peak. In order to obtain different concentrations in the cavity, heptane and acrylonitrile are injected into the mixing chip from inlets A and B at different injection rates controlled by the two programmable syringe pumps. Then, they were mixed thoroughly in the serpentine channel of the chip. In order to facilitate the acquisition of vibrational polaritons, the flow rate in the cavity is kept below 10 µm/min. As can be seen, when the acrylonitrile concentration was varied from 1.5 to 15 M, the Rabi splitting energy increased from 12.9 cm^{-1} to 38.6 cm^{-1}. A linear relationship between the Rabi splitting energy and the square root of the molecular concentration can be found, in agreement with the theoretical prediction (Eq. 4).

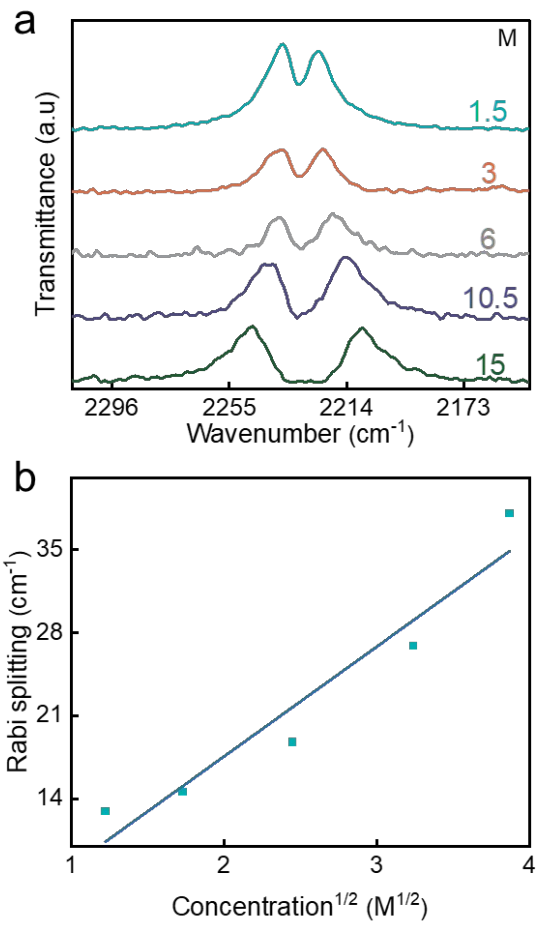

Figure 6. (a) Transmission spectra of an acrylonitrile-filled cavity at different concentrations (1.5-15 M). (b) Linear dependence of Rabi splitting and the square root of the acrylonitrile concentration, R=0.91.

Polariton dispersion

Figure S6a shows the transmission spectra of the vibrational polaritons recorded with an acrylonitrile-filled cavity with a light incident angle varying from 0 to 10° and the corresponding polariton dispersion curves at a step of 2°. The dispersion of the cavity mode and the vibrational mode of C≡N bond are also plotted. The angle-dependent polariton

dispersion can be fitted by using the following 2 × 2 Hamiltonian of coupled harmonic oscillators[43]

$$H=\begin{pmatrix}\tilde{\nu}_c(\theta) & \Omega_R/2\\ \Omega_R/2 & \tilde{\nu}_v\end{pmatrix} \quad (9)$$

where θ is the angle of the incident light to the cavity, $\tilde{\nu}_c$ is the photon energy of the cavity (in wavenumber unit), $\tilde{\nu}_v$ is the energy of the vibrational mode of the C≡N bond, and Ω_R the Rabi splitting parameter. By using Eq. 9 and the angle-dependent cavity photon energy,

$$\tilde{\nu}_c(\theta)=\tilde{\nu}_m\left(1-\frac{\sin^2\theta}{n_S^{\,2}}\right)^{-1/2} \quad (10)$$

the angle dispersion of the two polaritons can be determined. From the experimental data, we assign a cavity mode of order $m=6$ for the vibrational mode of $\tilde{\nu}_v$ = 2208 cm^{-1}. Then, the polariton dispersions can be fitted, as shown in Fig. S6b.

Technically speaking, the method developed in this work is more flexible and versatile compared to the conventional approaches using stainless steel cells and Mylar spacer. Considering the advantage of microfluidic techniques, VSC with a large number of molecules can be studied more conveniently by using this method. More generally, the microfluidic techniques can also be used to study other types of polaritons such as phonon-polariton, exciton-polariton, surface plasmon-polariton, magnon-polariton, etc.

Actually, the vibrational polaritons have attracted a growing interest for both fundamental research and synthetic chemistry. Important issues in cavity quantum electrodynamics including the effects of vacuum electromagnetic fields, coherent energy transfer, polariton dark states, polariton disordering, in collative relaxation, and polariton nonlinearity can be investigated in the framework of VSC.[2] Furthermore, open issues such as the possibility of quantum bits manipulation in a VSC system might be addressed.

We would like to mention that the system developed in this work is for proof of the concept and it can be improved for more systematic investigations. Firstly, the pressure drop across the cavity chip of this system was too high which may result in inhomogeneous deformation of the PDMS spacer. This can be avoided by adding an element or simply a tube of higher flow resistance downstream of the cavity chip so that the pressure drop will occur mainly in this part while the pressure in the chip area will be high and more homogeneous. Secondly, advanced microfluidic techniques such as hydrodynamic focusing can be introduced to generate more complex molecule systems. The microfluidic chip technologies are compatible with MEMS, surface patterning, and integrated sensing technologies, allowing further improvement the system. Finally, a FTIR spectrometer has been used in this work for easy implementation of the setup but it is limited in many aspects such as slow data acquisition and difficulty to perform both transmittance and reflectance. A dedicated setup might be built up by using such as quantum cascade lasers or free electron lasers to gain more freedoms in system design, and fast and multibeam recording.

Conclusions

We developed a microfluidic setup for convenient investigation of vibrational polaritons under a vacuum-strong coupling regime. We demonstrated that the fine-tuning of the cavity mode and the vibro-cavity mode coupling can be done by changing either the applied voltage to the piezoelectric actuators withstood the cavity or the flowrate of the solution in the cavity. We also demonstrated a linear dependence of the Rabi splitting on the square root of the molecular concentration by using two programmable syringe pumps. Acrylonitrile solutions were used in this work but many other molecular systems can also be used to investigate the vibrational polaritons and the chemical consequences of the VSC thanks to the robustness, flexibility, and versatility of the present method.

Acknowledgment

W.W. is supported by the Chinese Scholarship council. This work was supported by the French National Research Agency ANR (ANR-19-CE18-0009)

Author contributions

W.W. and Y.C. developed the microfluidic setup. W.W. performed the measurement and wrote the manuscript. J.F.D, N.D, and J.P. assisted the work and analyses. R.P., R.V. and Y.C. revised the manuscript. All authors contributed to discussions.

Additional information

Supplementary information is available for this paper.

Data availability

All data generated or analyzed during this study are included in this published article (and its supplementary information files).

References

1 T. W. Ebbesen, *Acc. Chem. Res.*, 2016, **49**, 2403–2412.
2 W. Xiong, *Acc. Chem. Res.*, 2023, **56**, 776–786.
3 H. Bahsoun, T. Chervy, A. Thomas, K. Börjesson, M. Hertzog, J. George, E. Devaux, C. Genet, J. A. Hutchison and T. W. Ebbesen, *ACS Photonics*, 2018, **5**, 225–232.
4 K. S. Menghrajani, H. A. Fernandez, G. R. Nash and W. L. Barnes, *Advanced Optical Materials*, 2019, **7**, 1900403.
5 L. Chuntonov, *Science*, 2022, **378**, 712–712.
6 J. George, A. Shalabney, J. A. Hutchison, C. Genet and T. W. Ebbesen, *J. Phys. Chem. Lett.*, 2015, **6**, 1027–1031.
7 J. George, T. Chervy, A. Shalabney, E. Devaux, H. Hiura, C. Genet

and T. W. Ebbesen, *Phys. Rev. Lett.*, 2016, **117**, 153601.
8 G. Khitrova, H. M. Gibbs, M. Kira, S. W. Koch and A. Scherer, *Nature Phys*, 2006, **2**, 81–90.
9 S. Aberra Guebrou, C. Symonds, E. Homeyer, J. C. Plenet, Yu. N. Gartstein, V. M. Agranovich and J. Bellessa, *Phys. Rev. Lett.*, 2012, **108**, 066401.
10 L. Shi, T. K. Hakala, H. T. Rekola, J.-P. Martikainen, R. J. Moerland and P. Törmä, *Phys. Rev. Lett.*, 2014, **112**, 153002.
11 A. D. Dunkelberger, B. T. Spann, K. P. Fears, B. S. Simpkins and J. C. Owrutsky, *Nat Commun*, 2016, **7**, 13504.
12 A. Sau, K. Nagarajan, B. Patrahau, L. Lethuillier-Karl, R. M. A. Vergauwe, A. Thomas, J. Moran, C. Genet and T. W. Ebbesen, *Angewandte Chemie International Edition*, 2021, **60**, 5712–5717.
13 A. Shalabney, J. George, J. Hutchison, G. Pupillo, C. Genet and T. W. Ebbesen, *Nat Commun*, 2015, **6**, 5981.
14 A. D. Wright, J. C. Nelson and M. L. Weichman, *J. Am. Chem. Soc.*, 2023, **145**, 5982–5987.
15 J. A. Campos-Gonzalez-Angulo, R. F. Ribeiro and J. Yuen-Zhou, *Nat Commun*, 2019, **10**, 4685.
16 M. Du, R. F. Ribeiro and J. Yuen-Zhou, *Chem*, 2019, **5**, 1167–1181.
17 J. Galego, C. Climent, F. J. Garcia-Vidal and J. Feist, *Phys. Rev. X*, 2019, **9**, 021057.
18 I. Vurgaftman, B. S. Simpkins, A. D. Dunkelberger and J. C. Owrutsky, *J. Phys. Chem. Lett.*, 2020, **11**, 3557–3562.
19 F. J. Hernández and F. Herrera, *The Journal of Chemical Physics*, 2019, **151**, 144116.
20 T. S. Haugland, C. Schäfer, E. Ronca, A. Rubio and H. Koch, *The Journal of Chemical Physics*, 2021, **154**, 094113.
21 M. V. Imperatore, J. B. Asbury and N. C. Giebink, *The Journal of Chemical Physics*, 2021, **154**, 191103.
22 G. D. Wiesehan and W. Xiong, *The Journal of Chemical Physics*, 2021, **155**, 241103.
23 K. Nagarajan, A. Thomas and T. W. Ebbesen, *J. Am. Chem. Soc.*, 2021, **143**, 16877–16889.
24 K. Joseph, S. Kushida, E. Smarsly, D. Ihiawakrim, A. Thomas, G. L. Paravicini-Bagliani, K. Nagarajan, R. Vergauwe, E. Devaux, O. Ersen, U. H. F. Bunz and T. W. Ebbesen, *Angewandte Chemie International Edition*, 2021, **60**, 19665–19670.
25 B. S. Simpkins, A. D. Dunkelberger and I. Vurgaftman, *Chem. Rev.*, 2023, **123**, 5020–5048.
26 K. Hirai, H. Ishikawa, T. Chervy, J. A. Hutchison and H. Uji-i, *Chemical Science*, 2021, **12**, 11986–11994.
27 J. George and J. Singh, *ACS Catal.*, 2023, **13**, 2631–2636.
28 K. Hirai, H. Ishikawa, Y. Takahashi, J. A. Hutchison and H. Uji-i, *Chemistry – A European Journal*, 2022, **28**, e202201260.
29 K. E. Mochalov, I. S. Vaskan, D. S. Dovzhenko, Y. P. Rakovich and I. Nabiev, *Review of Scientific Instruments*, 2018, **89**, 053105.
30 H. Hiura, A. Shalabney and J. George, *chemRxiv:*2019, 7234721.
31 J. Lather, P. Bhatt, A. Thomas, T. W. Ebbesen and J. George, *Angewandte Chemie International Edition*, 2019, **58**, 10635–10638.
32 Y. Chen, A. Tredicucci and F. Bassani, *Phys. Rev. B*, 1995, **52**, 1800–1805.
33 H. H. Li, *Journal of Physical and Chemical Reference Data*, 1980, **9**, 161–290.
34 R. L. Olmon, B. Slovick, T. W. Johnson, D. Shelton, S.-H. Oh, G. D. Boreman and M. B. Raschke, *Phys. Rev. B*, 2012, **86**, 235147.
35 E. Mohammad, *International Journal of Physics and Applications*. 2013, 47–57.
36 N. J. Hestand and F. C. Spano, *Acc. Chem. Res.*, 2017, **50**, 341–350.
37 J. M. Raimond, M. Brune and S. Haroche, *Rev. Mod. Phys.*, 2001, **73**, 565–582.
38 R. Houdré, R. P. Stanley and M. Ilegems, *Phys. Rev. A*, 1996, **53**, 2711–2715.
39 P. Törmä and W. L. Barnes, *Rep. Prog. Phys.*, 2014, **78**, 013901.
40 V. Savona, L. C. Andreani, P. Schwendimann and A. Quattropani, *Solid State Communications*, 1995, **93**, 733–739.
41 T. Gervais, J. El-Ali, A. Günther and K. F. Jensen, *Lab on a Chip*, 2006, **6**, 500–507.
42 H. Bruus, *Lab Chip*, 2011, **11**, 3742–3751.
43 M. S. Skolnick, T. A. Fisher and D. M. Whittaker, *Semicond. Sci. Technol.*, 1998, **13**, 645.